Journal of Power Sources 231 (2013) 23–28

Contents lists available at SciVerse ScienceDirect

Journal of Power Sources

journal homepage: www.elsevier.com/locate/jpowsour

Tailoring of phase composition and morphology of TiO_2-based electrode materials for lithium-ion batteries

M. Fehse [a,*], F. Fischer [b], C. Tessier [b], L. Stievano [a], L. Monconduit [a]

[a] ICG-AIME, UMR 5253, Université Montpellier 2, CC 1502, Place E. Bataillon, 34095 Montpellier Cedex 5, France
[b] SAFT, Direction de la Recherche, 111-113 Bd Alfred Daney, 33074 Bordeaux, France

HIGHLIGHTS

- Wide range of morphology and phase composition by adjusting two synthesis parameters.
- Tailoring of phase composition by adjusting alkalinity of hydrothermal synthesis.
- Tailoring of morphology in hydrothermal synthesis by adjusting powder concentration.
- Monoclinic TiO_2(b) phase shows higher rate capability than anatase phase.
- Higher internal resistance of anatase compared to TiO_2(b) is detected.

GRAPHICAL ABSTRACT

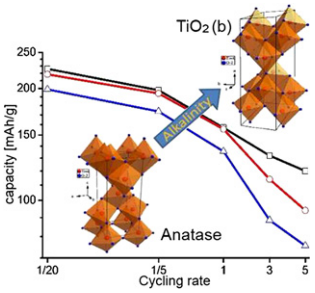

ARTICLE INFO

Article history:
Received 14 September 2012
Received in revised form
11 December 2012
Accepted 14 December 2012
Available online 27 December 2012

Keywords:
TiO_2 anatase
TiO_2(b)
Hydrothermal synthesis
Lithium ion batteries (LIB)
Reversible capacity

ABSTRACT

Titanium dioxide mixed phases containing TiO_2(b) and anatase phase in different ratios were prepared via a facile, template free, low temperature hydrothermal synthesis. Morphology and phase composition were tuned by adequately adjusting the main synthesis parameters, i.e., temperature, powder/liquid ratio and basicity of the mother solution. The effect of different phase compositions on the lithium insertion and de-insertion properties was tested by electrochemical cycling at increasing cycling rates. Results indicate a superiority of monoclinic TiO_2(b) phase over the tetragonal anatase phase especially at elevated cycling rates. Further analysis shows that internal resistance is one of the major limitations for electrochemical cycling of anatase.

1. Introduction

Lithium ion batteries (LIB) are today's leading and commercially well established batteries for high power applications. Their high energy density, low memory effect and wide working temperature range make them superior over other battery materials. Continuous research and development ever since its introduction to the market in the early 90's by *SONY* has lead to their wide spreading in numerous applications [1,2]. The current anode material of choice is graphite which features good lithium insertion properties and is easily available throughout the world. However, technological progress demands for faster, safer, lighter and higher capacity battery materials. TiO_2 is equally environmentally benign and cost effective but has superior safety and rate capability compared with

* Corresponding author. Tel.: +33 467149099; fax: +33 467143304.
E-mail addresses: mfehse@um2.fr, marcus.fehse@gmail.com (M. Fehse).

0378-7753/$ – see front matter © 2012 Elsevier B.V. All rights reserved.
http://dx.doi.org/10.1016/j.jpowsour.2012.12.058

graphite [3]. The latter is due to unrestrictedness of ion flow hence significantly higher charge and discharge rates are possible. Its elevated working potential of ≈1.5 V constitutes not only an inherent lithium overcharge protection but also suits conveniently the thermodynamic stability window of common organic electrolytes [4]. The spinel type titania $Li_4Ti_5O_{12}$ is considered as reference material for titania materials in battery applications. It has relatively low theoretical capacity of 175 mAh g^{-1} but proves to be very stable in practical application [5,6]. The most extensively studied TiO_2 phase regarding feasibility as lithium insertion material is anatase. It has a theoretical capacity of 336 mAh g^{-1} corresponding to the insertion of one mol lithium per one mol of TiO_2. In practice however only half of that value is obtained since insertion exceeding 0.5 Li per unit cell TiO_2 imposes severe structural changes in the bulk material from tetragonal to orthorhombic phase [7].

One of the most vividly discussed approaches to increase the capacity of titania is nanostructuring. Using nanoscaled particles as an active lithium insertion material not only offers the opportunity to overcome the low electron and ion conductivities imposed by bulk structure but also enhances rate and cycling performance by increasing electrode–electrolyte contact area and surface to volume ratio. Such an open and unconfined structure permits higher diffusion rates due to surface diffusion as well as easy accessibility.

More recently the monoclinic phase of titania, TiO_2(b) has received increased attention. It has one of the lowest densities of all titania polymorphs [8] expressed by a more open structure which is believed to facilitate internal lithium migration [5,9] and consequently leads to superior rate capabilities. Various studies indicate such a superiority of cycling performance [10,11]. The latter of which attributes this superiority to a pseudocapacitive storage that is based on unique sites as well as on particular diffusion and absorption energetics of TiO_2(b) [12]. TiO_2(b)'s ability to store significant amounts of lithium in surface region is a promising asset for high performance application.

Hydrothermal synthesis is very appealing because of its feasibility for application in industry. It is not only cost effective but it also can be scaled up easily. Furthermore it proves to be a versatile approach to produce a broad variety of morphologies without the help of template or surfactant. Pioneering work on hydrothermal synthesis of anatase nanotubes was done by Kasuga et al. [13]. Later this method was adopted by Bruce et al. for hydrothermal preparation of TiO_2(b) nanowires [9].

In this study we show a facile and cost effective method of producing nanoscaled TiO_2 with tunable morphology and phase composition. Moreover we give insights on how these material characteristics influence key factors of electrochemical cycling such as rate capability, capacity retention and coulombic efficiency.

2. Experimental details

2.1. Synthesis

The mixed titania phases were synthesized via hydrothermal treatment in alkaline environment based on procedure by Yoshida et al. [14]. As starting material TiO_2 from *Umicore* was used which was mixed with NaOH in distilled water. Throughout stirring a homogeneous solution was obtained which was transferred into a Teflon lined autoclave and kept at 150 °C for 72 h. After cooling naturally to ambient temperature the white, sorbet-like product was washed in distilled water to eliminate remaining NaOH before washing in 0.1 M HCl at pH ≤ 2. In a final washing step the solution was brought to neutrality. Subsequently the product was dried at ≈100 °C, ground and sieved to a 50 μm mesh. In a final preparation step the white powder samples were heat treated in air at 450 °C for 4 h in air. The experimental procedure is shown in a simplified flow chart, see Fig. 1.

2.2. Electrode and cell preparation

For electrochemical measurements the synthesized titania powder was mixed with carbon black and PVDF with a weight composition of 80:8:12, respectively. An NMP-based slurry of this mixture was tape casted on copper foil using a doctor blade system and used as working electrode. These were built in *Swagelok* cells together with lithium metal as reference and counter electrode as well as *Whatman* fiber glass separators. A mixture of organic solvents containing ethylene carbonate, propylene carbonate and dimethyl carbonate in composition 1:1:3 and 1 M $LiPF_6$ was used as electrolyte. Since electrolyte and lithium metal are very sensitive to air and moisture, the assembly of the electrochemical cells was carried out in glove box under Ar atmosphere.

2.3. Characterization

Electrochemical cycling was carried out in galvanostatic mode on *Biologic* multichannel potentiostat. Different cycling rates were applied ranging from C/20 to 5C whereas 1C is equal to a current of 336 mA g^{-1}. The crystal structures were defined via powder X-ray diffraction (XRD) using *Philips Expert* with Cu Kα radiation at room temperature spectra ranging from 10 to 70° with step size of 0.00334°. Raman spectroscopy was carried using *LabRam ARAMIS IR*^{2}, *Horiba Jobin Yvon* with blue diode laser $\lambda = 473$ nm or helium neon laser $\lambda = 633$ nm. Nitrogen physisorption was carried out on a *Micromeritics ASAP2020* and analyzed using BET as well DFT methods to calculate specific surface area and pore size distribution, respectively. The morphological characterization was conducted using TEM pictures taken with *JOEL 1200EXS* and *SIS Olympus Quemesa* camera.

The phase composition calculation is based on peak area retrieved from XRD data. Characteristic and distinct peaks for each phase were chosen, fitted and compared. For XRD the (200) and (003) reflections for TiO_2(b) as well (004) and (211) for anatase phase respectively were selected. The calculated values are in agreement within 10% deviation with the values obtained from

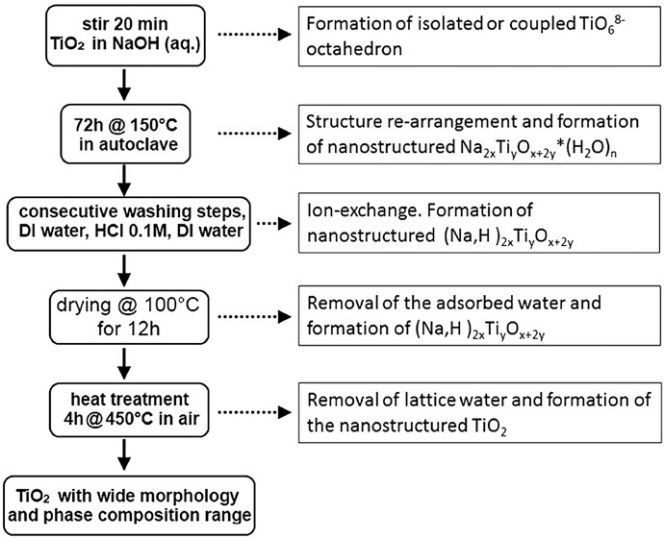

Fig. 1. Flow chart of hydrothermal synthesis for tailored TiO_2 polymorph, mixed phases.

parallel calculations performed on the base of Raman spectra. For the latter the mutual peak of anatase and TiO_2(b) at 146 cm^{-1} was compared with intensity that of the TiO_2(b) specific peak at 121 cm^{-1}, as proposed by Beuvier et al. [15].

3. Results

3.1. Hydrothermal synthesis

Throughout a comprehensive survey of hydrothermal synthesis we were able to define dependencies and trends, at a defined synthesis temperature, regarding morphology and structure of the obtained titania. An overview of the different morphologies that could be obtained throughout facile adjusting of the powder concentration in the mother solution is given in Fig. 2. It shows the nitrogen physisorption curves and TEM pictures of the three main morphology groups. All physisorption isotherm follow the same pattern which is defined as type II curve by *UIPAC* [16] which connotes monolayer and multilayer adsorption on non-porous materials. The opening of hysteresis at pressure above $p/p_0 \approx 0.8$ and extending up to $p/p_0 \approx 1$ states that only large pores are present which are not all filled. This is in agreement with the TEM pictures which show no small pores inside the particles. The large pores correspond to the spaces between the aggregates, whereas the nanoparticle morphology shows the highest content of such inter-particle voids. The strong difference of the quantity of absorbed nitrogen is directly linked to the specific surface area, which ranges from 250 m^2 g^{-1} for sheet, 190 m^2 g^{-1} for nanoparticles and 50 m^2 g^{-1} for rod structure.

Experimentally we find that for high concentration of titania corresponding to a log (Na/Ti) value below 0.9 a sheet structure favored while decrease in concentration toward a log (Na/Ti) value of 1 leads to elongated nanoparticles with average diameter of ≈15 nm. As we further dilute the titania in mother solution these rods grow bigger and at 1.3 are composed almost entirely of ribbons or rods with average diameter of 40–60 nm. The latter is the most commonly found morphology for these synthesis conditions and has been published by many groups before [9,14,17–19]. To the best of our knowledge sheet structures are however seldomly obtained throughout this kind of synthesis. Usually the dehydration during drying process is coupled to the formation of cage and tubular structures [20–22]. Presumably a low concentration (log (Na/Ti) value) suppresses this formation and hence micrometer scale TiO_2 sheets are preserved.

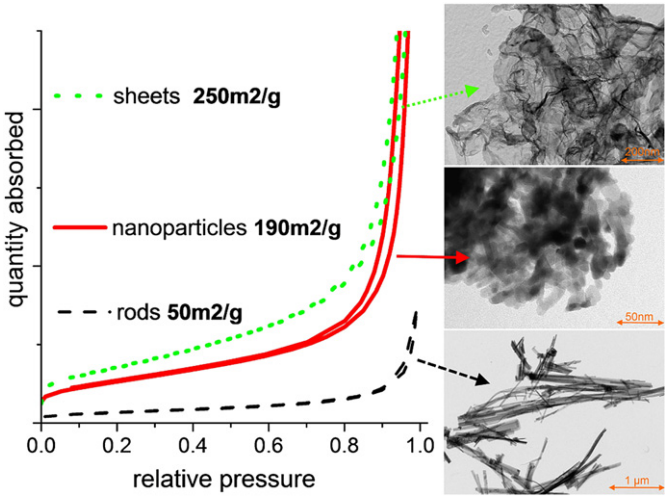

Fig. 2. Nitrogen physisorption curves and TEM pictures of three main morphologies; sheets, nanoparticles and rods synthesized throughout adequately adjusting powder concentration in the mother solution.

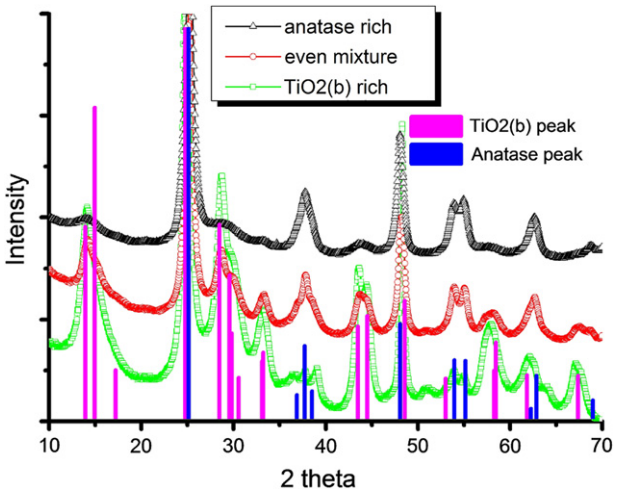

Fig. 3. XRD pattern of three biphasic TiO_2 mixtures containing different ratios of anatase and TiO_2 (b) phase.

In Fig. 3 the XRD patterns of three selected samples with different phase compositions are compared. The low signal-to-noise-ratio denotes a partial crystallization while the broadened peaks indicate very small crystallite sizes. These circumstances in combination with the fact of similar reflex positions of anatase (ICSD 9852) and TiO_2(b) (ICSD 171670) [23] make Raman an indispensable characterization method for distinguishing and quantifying these phases [15], see Fig. 4. The Anatase-to-TiO_2(b) ratio ranges from anatase rich 80/20 over even mix 40/60 to TiO_2(b)rich 10/90 sample. We found that at 150 °C, a NaOH concentration lower than 11 M produces mainly anatase, whereas higher concentrations lead to samples rich in TiO_2(b) which is in good agreement with findings by Armstrong et al. [9]. It should be noted that the XRD and TEM study of the samples before the final heat treatment (not shown) reveals that the phase composition is globally preserved, displaying that the latter step only produces a dehydration of the solid and does not influence the structure. Furthermore we like to point out the difficulties of obtaining pure phases by this synthesis method while maintaining the morphology. This limitation arises from an interdependence of the two main synthesis parameters, powder concentration and alkalinity.

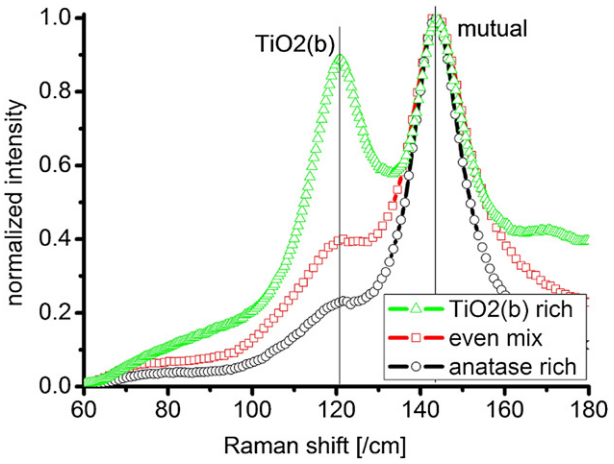

Fig. 4. Raman spectra of three biphasic TiO_2 mixtures containing different ratios of anatase and TiO_2 (b) phase.

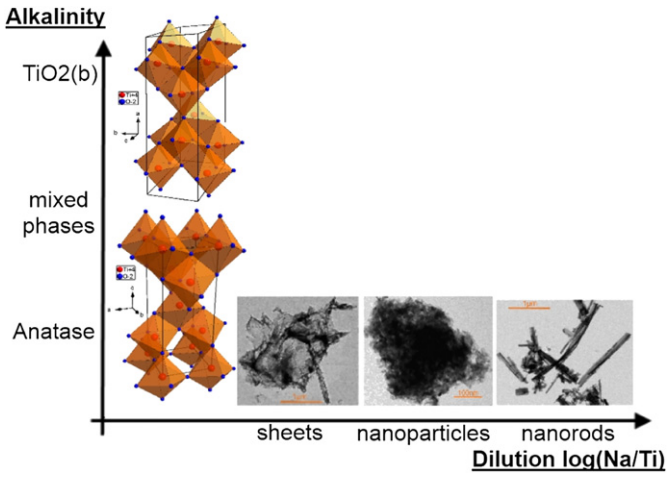

Fig. 5. Trends and dependencies found for hydrothermal synthesis of regarding phase composition and morphology of titania. Increasing dilution (Na/Ti ratio) leads from a) sheets to b) elongated nanoparticles and finally to c) developed nanorods/nanoribbons while increasing the pH promotes TiO_2(b) formation.

In summary it can be stated that while the alkalinity is mainly influencing the phase composition in terms of anatase/TiO_2(b) ratio, the concentration (Na/Ti ratio) affects primarily the morphology of the resulting titanate. These trends are condensed in Fig. 5 which features TEM images of the variety of different morphologies obtained sheets, nanoparticles and rods as well as structural models of the tetragonal TiO_2 anatase and monoclinic TiO_2(b) phase. This figure shows imposingly that a wide range of morphologies and phase compositions can be achieved throughout the simple adjustment of two synthesis parameters of the hydrothermal synthesis. This approach for tailoring TiO_2 is an attractive alternative to the use of template or surfactants which often are costly, toxic, hazardous or are difficult to remove without residue.

3.2. Electrochemical cycling

Tape casting resulted in homogeneous, uniform and smooth film electrodes with loading of roughly 1.5 mg cm^{-2}, see Fig. 6. In this figure one can well distinguish between the nanoribbons of TiO_2(b) active material and the spherical carbon black particles.

Three samples were chosen for electrochemical characterization which feature different phase composition but similar nanorod morphology. An anatase rich sample (80/20), a mix composition sample (40/60) and a TiO_2(b) rich sample (10/90) with specific surface areas of 180, 70 and 50 $m^2\ g^{-1}$ respectively were tested. In Fig. 7 the galvanostatic curve of the first two cycles are pictured for a) TiO_2(b) rich sample (10/90), b) even mix (40/60) and c) anatase rich sample (80/20). When comparing the electrochemical cycling curves one notices that while TiO_2(b) rich sample shows a continuously decreasing "S"-shaped slope, the anatase rich sample has first a characteristic plateau at roughly 1.8 V up to 0.3 Li which is then followed by a slope like insertion, which is in accordance with

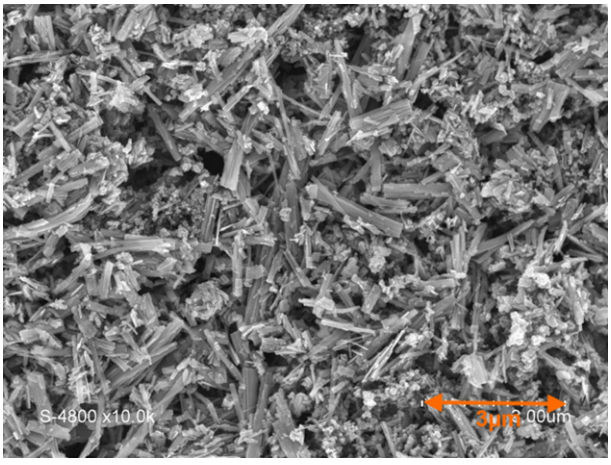

Fig. 6. SEM picture at 10 k magnification of TiO_2(b) rich electrode film.

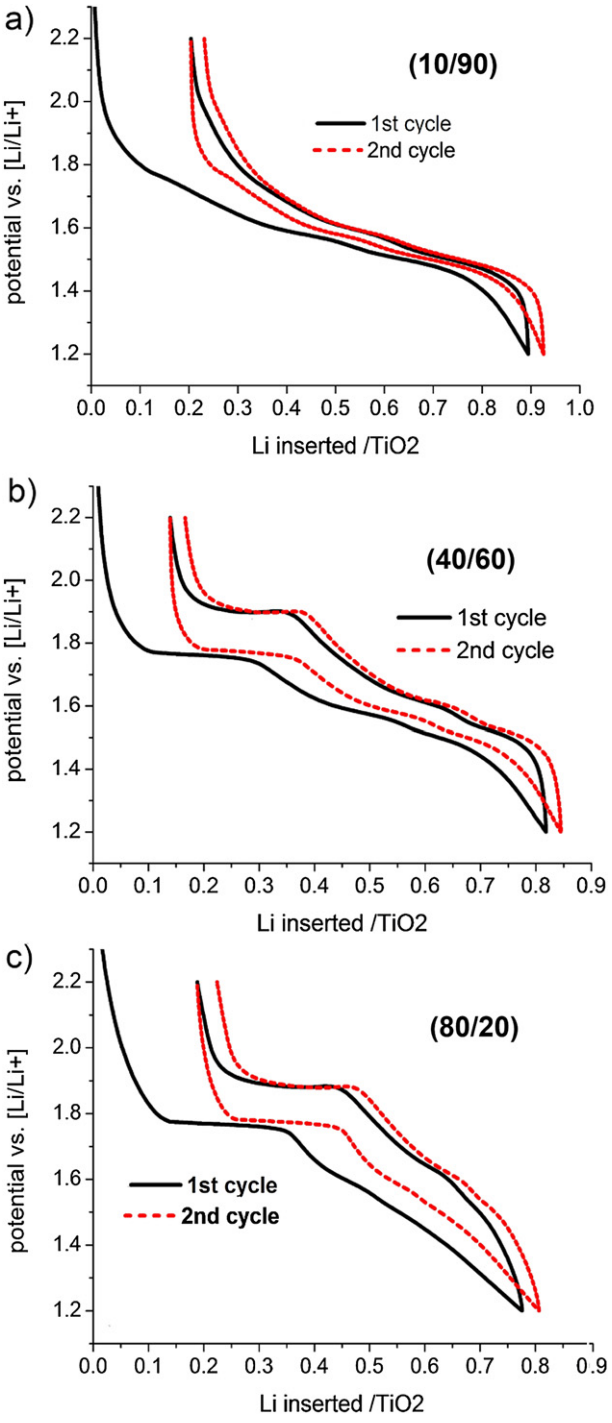

Fig. 7. Potential as function of number of lithium inserted for the first two galvanostatic cycles of titania nanorod samples with anatase-to-TiO_2(b) ratio of (a) 10/90 (b) 40/60 and (c) 80/20.

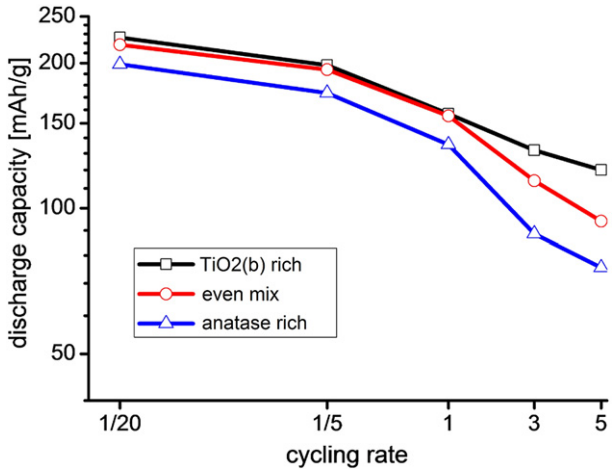

Fig. 8. Evolution of capacities for samples of high (80/20), medium (60/40) and low content (10/90) content of anatase as function of cycling rate.

literature data in [3,15,24] and [19,25], respectively. The even mix sample shows similar behavior but with a shorter plateau compared to the anatase-rich sample. These differences agree with the fact that, although anatase and TiO_2(b) are chemically similar, lithium insertion and de-insertion reaction follow different mechanisms. The capacity loss between first and second cycle is a frequently seen phenomena for TiO_2 materials. For the three samples here investigated a capacity loss of ≈20% was found regardless of their specific surface area differences or phase phase composition. This low coulombic efficiency is attributed in the literature either to the electrolyte decomposition induced formation of a solid electrolyte interphase (SEI) and/or filling of irreversible lithium sites in the TiO_2 structure [4,5,15,25,26]. Currently carried out experiments to investigate the origin of this phenomena are indicating a degradation of certain electrolyte components occurring at potential values far above SEI formation potentials within their supposed stability window. This might be related to catalytic effect due to the presence of high specific surface area nanostructured TiO_2. However this is only a suspicion and further measurements will be necessary to shed light on this curiosity.

To evaluate the rate capability and capacity retention of the samples several consecutive cycling runs with the same cell while progressively increasing the cycling rate were carried out which leads to a step function behavior (not shown). To facilitate the comparison of their electrochemical storage ability the mean capacities of the 10th cycle as function of cycling rate for the three samples with different phase composition are plotted in Fig. 8. This graph reveals an inverse relation between cycling speed and capacity obtained. Although this is a mutual trend for three investigated samples significant differences were found.

The mutual trend of reducing capacities as cycling speed is increased, can be attributed to growing kinetic limitations. At the low cycling rate of C/20 capacity values of different phase composition lie between 200 and 220 mAh g^{-1}. However the capacities obtained for anatase rich and even mixture sample decrease stronger than the capacities of TiO_2(b) rich sample once the cycling rate is accelerated. At 5C anatase rich sample and even mixture sample reach only ≈70 mAh g^{-1} and 95 mAh g^{-1}, respectively while for TiO_2(b)-rich sample 120 mAh g^{-1} was obtained. This result is in line with the general idea that the anatase phase is less capable of lithium ion insertion and de-insertion at elevated rates than the bronze phase [3,11,12,27]. Such superior performance of TiO_2(b) is in agreement with values of literature 190 mAh g^{-1} at 0.65C and 100 mAh g^{-1} at 6C [5], 202 mAh g^{-1} at 0.65C and 140 mAh g^{-1} at 6C [28] as well as 175 mAh g^{-1} at C/3 and 75 mAh g^{-1} at 6C [15]. Naturally these values can only be taken as a rough orientation for comparison since key factors such as electrode formulation and preparation, specific surface area and electrode loading are staggering.

In order to further elucidate this phenomena we have studied the derivative curves of the galvanostatic cycling which allows to determine not only the exact electrochemical potential of lithium ion insertion and de-insertion reaction of the anatase and TiO_2(b) phase but also estimate their intensity (peak area). In Fig. 9 two derivative curves of an even mixture sample (40/60) are presented cycled a) at C/20 and b) 5C. Characteristic twin peaks of TiO_2(b) at ≈1.5 V are identified as well as the anatase contribution at ≈1.8 V [29].

Two things are salient when comparing the derivatives at different cycling rates. Firstly the proportion changes of the peaks corresponding to the reaction of anatase and of the TiO_2(b) phase. While anatase peaks are striking at C/20 they are faint at 5C. Secondly a smaller shift of the peak position for TiO_2(b) than for anatase is found which is shown in Fig. 10 for an even mixture sample (60/40). The potential shift was calculated by subtracting the reduction potential (Li insertion) from the oxidation potential (Li de-insertion), taken from the derivative curve. This indicates that anatase compared to TiO_2(b) bears higher internal resistance which is in line with the superior rate capability of TiO_2(b) stated in Fig. 8. This leads us to the conclusion that that anatase phase is less suitable for high performance cycling than TiO_2(b) phase.

Although chemically equal, anatase and TiO_2(b) feature different electronic and crystal structure which determine not only the diffusion rates but also the position, accessibility and energetics of lithium insertion sites [12,18,25,30–33]. In this lies the reason for the strong deviation between redox potentials of lithium insertion

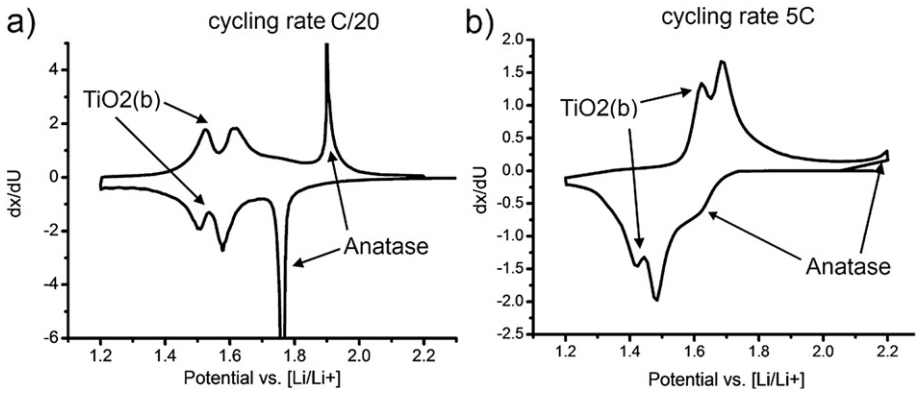

Fig. 9. Derivative curves of an even mix sample at a) C/20 and b) 5C. Characteristic lithium insertion and de-insertion peaks of the two coexisting phases are marked.

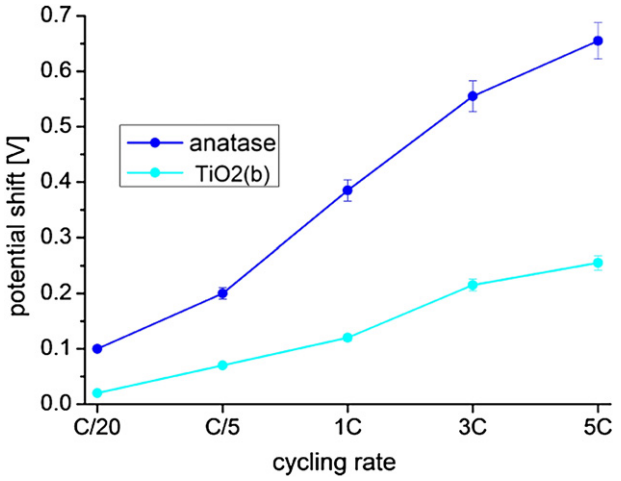

Fig. 10. Shift redox potential as function of cycling rate for the anatase and TiO_2(b) phase component of even mixture (40/60) sample including standard deviation.

and de-insertion of the anatase and TiO_2(b) phase as well as the distinct differences in polarization of the two phases.

4. Conclusions

Successful tailoring of both morphology and phase composition of TiO_2 was obtained via facile hydrothermal synthesis in alkaline environment without application of any template or surfactant. In electrochemical cycling experiments such samples achieved respectable capacities exceeding 220 mAh g^{-1} with good capacity retention at low cycling rate. Cycling results at progressively increased cycling rate reveal a superior rate capability of samples with elevated content of monoclinic TiO_2(b) phase. Comparative study of the evolution of the redox potentials of the two TiO_2 phases shows a diverging polarization of anatase and TiO_2(b) phase with increasing cycling rate. Our studies confirm the feasibility of TiO_2(b) as candidate for lithium insertion material for high power application while also pointing out the necessity to investigate the insertion mechanism of TiO_2(b) in detail as it seems to be significantly different from the well studied anatase phase. Currently carried out in situ experiments are aimed at deepening our understanding on the origin of the here claimed superiority of TiO_2(b) over anatase phase.

Acknowledgments

The authors are grateful for financial support by *Saft* and *CNRS*. Furthermore we wish to thank the anonymous reviewers for their valuable suggestions.

References

[1] Michael M. Thackeray, Sun-Ho Kang, Christopher S. Johnson, John T. Vaughey, Roy Benedek, S.A. Hackney, Journal of Materials Chemistry 17 (30) (2007) 3112.
[2] Tsutomu Ohzuku, Ralph J. Brodd, Journal of Power Sources 174 (2) (December 2007) 449–456.
[3] Yu Ren, Zheng Liu, Frédérique Pourpoint, A. Robert Armstrong, Clare P. Grey, Peter G. Bruce, Angewandte Chemie 124 (9) (February 2012) 2206–2209.
[4] Sergio Brutti, Valentina Gentili, Priscilla Reale, Lorenzo Carbone, Stefania Panero, Journal of Power Sources 196 (22) (November 2011) 9792–9799.
[5] A. Robert Armstrong, Graham Armstrong, Jesus Canales, Peter G. Bruce, Journal of Power Sources 146 (1–2) (2005) 501–506.
[6] Aurelien Du Pasquier, C.C. Huang, Timothy Spitler, Journal of Power Sources 186 (2) (January 2009) 508–514.
[7] R.J. Cava, D.W. Murphy, S. Zahurak, Journal of Solid State Chemistry 53 (1) (1984) 64–75.
[8] Zhenguo Yang, Daiwon Choia, Sebastien Kerisit, Kevin M. Rosso, Donghai Wang, Jason Zhang, Gordon Graff, Jun Liu, Journal of Power Sources 192 (2) (2009) 588–598.
[9] A. Robert Armstrong, Graham Armstrong, Jesús Canales, Peter G. Bruce, Angewandte Chemie, International Edition in English 43 (17) (April 2004) 2286–2288.
[10] Thierry Brousse, René Marchand, Pierre-Louis Taberna, Patrice Simon, Journal of Power Sources 158 (1) (July 2006) 571–577.
[11] Marketa Zukalova, Martin Kalbac, Ladislav Kavan, Ivan Exnar, Michael Graetzel, Chemistry of Materials 17 (2005) 1248–1255.
[12] M.V. Koudriachova, Surface and Interface Analysis 42 (December 2009) 1330–1332.
[13] Tomoko Kasuga, Masayoshi Hiramatsu, Akihiko Hoson, Toru Sekino, Langmuir 7463 (5) (1998) 3160–3163.
[14] Ryuhei Yoshida, Yoshikazu Suzuki, Susumu Yoshikawa, Journal of Solid State Chemistry 178 (2005) 2179–2185.
[15] Thomas Beuvier, Mireille Richard-Plouet, Maryline Mancini-Le Granvalet, Thierry Brousse, Olivier Crosnier, Luc Brohan, Inorganic Chemistry 49 (18) (September 2010) 8457–8464.
[16] K.S.W. Sing, Pure and Applied Chemistry 54 (11) (1982) 2201–2218.
[17] Min Gyu Choi, Young-Gi Lee, Seung-Wan Song, Kwang Man Kim, Electrochimica Acta 55 (20) (August 2010) 5975–5983.
[18] Toyoki Okumura, Tomokazu Fukutsuka, Asuki Yanagihara, Yuki Orikasa, Hajime Arai, Zempachi Ogumi, Yoshiharu Uchimoto, Journal of Materials Chemistry 21 (39) (2011) 15369.
[19] Jinwei Xu, Caihong Jia, Bin Cao, W.F. Zhang, Electrochimica Acta 52 (2007) 8044–8047.
[20] Guan-Nan Zhu, Cong-Xiao Wang, Yong-Yao Xia, Journal of Power Sources 196 (5) (March 2011) 2848–2853.
[21] Maurizio Casarin, Andrea Vittadini, Annabella Selloni, ACS Nano 3 (2) (February 2009) 317–324.
[22] Thomas P. Feist, Peter K. Davies, Journal of Solid State Chemistry 101 (1992) 275–295.
[23] Inorganic Crystal Structure Database (ICSD), FIZ Karlsruhe.
[24] A. Robert Armstrong, G. Armstrong, J. Canales, R. García, Peter G. Bruce, Advanced Materials 17 (7) (2005) 862–865.
[25] U. Lafont, D. Carta, G. Mountjoy, A.V. Chadwick, E.M. Kelder, The Journal of Physical Chemistry C 114 (2) (2010) 1372–1378.
[26] M. Pfanzelt, P. Kubiak, M. Fleischhammer, M. Wohlfahrt-Mehrens, Journal of Power Sources 196 (16) (August 2011) 6815–6821.
[27] Hansan Liu, Zhonghe Bi, Xiao-Guang Sun, Raymond R. Unocic, M. Parans Paranthaman, Sheng Dai, Gilbert M. Brown, Advanced Materials (Deerfield Beach, Fla.) 23 (30) (August 2011) 3450–3454.
[28] Jianming Li, Wang Wan, Henghui Zhou, Jingjian Li, Dongsheng Xu, Chemical Communications (Cambridge, England) 47 (12) (March 2011) 3439–3441.
[29] Yosuke Ishii, Yusuke Kanamori, Takehiro Kawashita, Indrajit Mukhopadhyay, Shinji Kawasaki, Journal of Physics and Chemistry of Solids 71 (4) (April 2010) 511–514.
[30] Corinne Arrouvel, Stephen C. Parker, M. Saiful Islam, Chemistry of Materials 21 (20) (2009) 4778–4783.
[31] Shaohua Liu, Haiping Jia, Lu Han, Jiulin Wang, Pengfei Gao, Dongdong Xu, Jun Yang, Shunai Che, Advanced Materials (Deerfield Beach, Fla.) 24 (May 2012) 3201–3204.
[32] B. Zachau-Christiansen, K. West, T. Jacobsen, Solid State Ionics 30 (1988) 1176–1182.
[33] Gerhard Nuspl, Kazyunari Yoshizawa, Tokio Yamabe, Journal of Materials Chemistry 7 (12) (1997) 2529–2536.